An affordable linkage-and-tendon hybrid-driven anthropomorphic robotic hand – MCR-Hand II

Yang, H, Wei, G, Ren, L, Qian, Z, Wang, K, Xiu, H and Liang, W

http://dx.doi.org/10.1115/1.4049744

An Affordable Linkage-and-Tendon Hybrid-Driven Anthropomorphic Robotic Hand – MCR-Hand II

Haosen Yang
Research Student
School of Mechanical, Aerospace and Civil Engineering
The University of Manchester
Manchester, M13 9PL, UK
Email: haosen.yang@postgrad.manchester.ac.uk

Guowu Wei*
Lecturer, Member of ASME
School of Science, Engineering and Environment
University of Salford
Manchester, M5 4WT, UK
Email: g.wei@salford.ac.uk

Lei Ren*
Reader
School of Mechanical, Aerospace and Civil Engineering
The University of Manchester
Manchester, M13 9PL, UK
Email: lei.ren@manchester.ac.uk

Zhihui Qian
Professor
Key Laboratory of Bionic Engineering, Ministry of Education
Jilin University
Changchun, 130025 P.R. China
Email: zhqian@jlu.edu.cn

Kunyang Wang
Lecturer
Key Laboratory of Bionic Engineering, Ministry of Education
Jilin University
Changchun, 130025 P.R. China
Email: kywang@jlu.edu.cn

Haohua Xiu
Research Associate
Key Laboratory of Bionic Engineering, Ministry of Education
Jilin University
Changchun, 130025 P.R. China
Email: xiuhh@jlu.edu.cn

Wei Liang
Research Student
Key Laboratory of Bionic Engineering, Ministry of Education
Jilin University
Changchun, 130025 P.R. China
Email: weiliang16@mails.jlu.edu.cn

ABSTRACT

This paper presents the design, analysis and development of an anthropomorphic robotic hand coined MCR-Hand II. This hand takes the advantages of both the tendon-driven and linkage-driven systems, leading to a compact mechanical structure that aims to imitate the mobility of a human hand. Based on the investigation of the human hand anatomical structure and the related existing robotic hands, mechanical design of the MCR-Hand II is presented. Then, using D-H convention, kinematics of this hand is formulated and illustrated with numerical simulations. Further, fingertip force is deduced and analysed, and mechatronic system integration and control strategy are addressed. Subsequently, a prototype of the proposed robotic hand is developed, integrated with low-level control system, and following which empirical study is carried out, which demonstrates that the proposed hand is capable of implementing the grasp and manipulation of most of the

*Address all correspondence to these authors.

objects used in daily life. In addition, the three widely used tools, i.e. the Kapandji score test, Cutkosky taxonomy and Kamakura taxonomy, are used to evaluate the performance of the hand, which evidences that the MCR-Hand II possesses high dexterity and excellent grasping capability; object manipulation performance is also demonstrated.

This paper hence presents the design and development of a type of novel tendon-linkage-integrated anthropomorphic robotic hand, laying broader background for the development of low-cost robotic hands for both industrial and prosthetic use.

1 INTRODUCTION

Human hand is the most important organ for adaptation and exploration of external environment, and for prehension, perception and manipulation of daily life tools and objects. Building an artificial hand which is capable of replicating the functionalities of human hand is a dream of human beings, especially for researchers and engineers in robotics research. The design and development of functional artificial hand can be traced back to the 'Berlichingen hand' in the 16th century and it has been over six decades since the modern research in robotic hand emerged [1]. A rather comprehensive review on the development of robotic hand in the past century was recently presented by Piazza et al. [2].

At the early stage, robotic hands were developed in the forms of grippers with specific functions for industrial applications [3], and functionally simplified anthropomorphic hands for prosthetics use (such as the Belgrade hand) [1, 4]. The Okada hand [5] and especially the later on Utah/MIT hand [6] were deemed to be cornerstone of the design and development of dexterous robotic hands. After these a great number of dexterous robotic hands have been proposed and presented [2]. One of the trends in the dexterous robotic hand research is to develop anthropomorphic robotic hand that can emulate or even replicate the function of human hand, aiming for the applications in complex and unstructured environment. These anthropomorphic robotic hands include, to mention but a few, the Hitachi Hand [7], the DIST hand [8], the Robonaut 1 [9] and 2 [10] hands, the DLR Hand I [11], II [12], and III [13], the Metamorphic hand [14–17] and the Shadow hand®. In the design of these anthropomorphic robotic hands including the underac-

tuated ones [18, 19], except for the recent development of soft-material-based anthropomorphic robotic hands (which provide better adaptability for dexterous grasping but actually lack of full versatile in-hand manipulability comparing to human hand) [20–22], a wide range of transmission systems including tendons, linkages, gear trains and belts were used. In these transmission systems, tendon and linkage systems are the two most commonly implemented transmissions. The tendon-driven robotic hands normally have the actuators located remotely from the joints, which helps reduce the weight and dimensions for the fingers. Examples of tendon-driven anthropomorphic robotic hands are the Stanford/JPL hand [23], the Utah/MIT hand [6], the Shadow hand®, the ACT hand [24] and the DEXMARThand [25]. The linkage-driven robotic hands provide better stiffness properties and allow bidirectional control, but in the meanwhile have greater weight and dimension of the fingers. The typical linkage-driven anthropomorphic robotic hands are the Gifu hand III [26], the NAIST Hand [27] and the Robonaut 2 hand [10]. It was noticed that either tendon-driven or linkage-driven method was implemented in design of the most of rigid-body-based anthropomorphic robotic hands, though there was rare case that combined both linkage and tendon driven methods. In the design of the Alpha hand [28] a linkage-driven actuation scheme was used for locating the fingers, and a under-actuated tendon-driven actuation scheme was employed for enhancing grasping force. In the CATCH-919 hand [29], linkage-based fingers were constructed that were actuated by tendon-driven scheme with linear springs providing mechanical compliance.

Further, it has been noticed that except for some prosthetic hands [30, 31], most of the anthropomorphic robotic hands are expensive due to the high costs of component fabrication, actuators, and sensory and control system; and thus applications of these robotic hands are limited. The emerging 3D printing technology has made the design and development of robotic hand convenient and affordable. Using such rapid prototyping technology, a great number of robotic hands have been presented [19, 25, 32], and a number of open-source initiatives such as the Open Hand Project [33] and the OpenBionics platform [34] were established for supporting such development.

In this paper, we aim to design a low-cost 3D-printed anthropomorphic robotic hand by using a linkage-and-tendon combined transmission system. Low-cost servomotors with sufficient driving power are used as actuators, integrated with economical micro-controller. The proposed

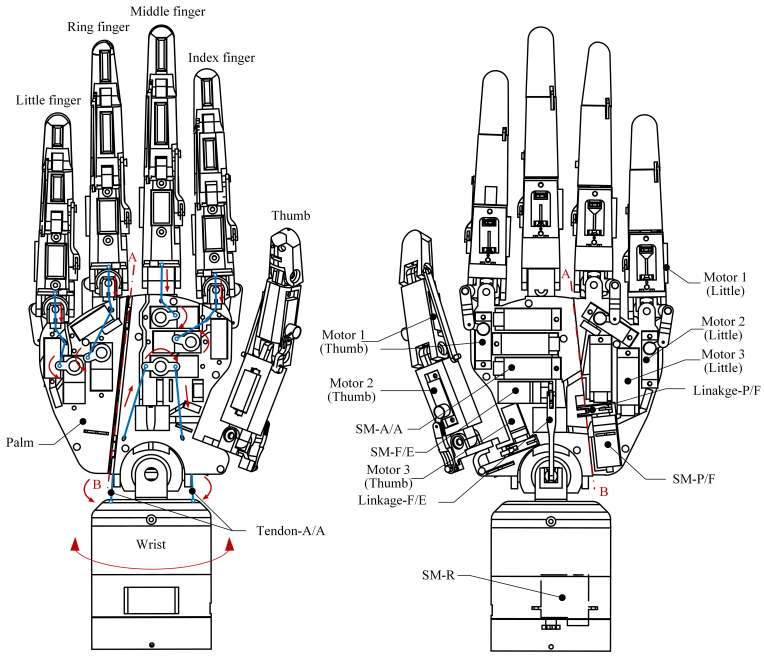

Fig. 1. The mechanical structure of the MCR-Hand II.

anthropomorphic hand is expected to be in the size of a human hand with a weight of less than 800g. All actuators will be embedded inside the fingers and palm. A compact 3-DoF wrist is also considered, providing space for accommodating the micro-controller and the associated electronic components, and in the meanwhile serving as a connector to robot arms.

The paper starts with mechanical design of the MCR-Hand II in Section II which is followed by the kinematics and force analysis in Section III. Section IV presents mechatronic system integration and control, and prototype, empirical study and evaluation are addressed in Section V. Conclusions for the proposed research is given in Section VI.

2 MECHANICAL DESIGN OF THE MCR-HAND II

2.1 Structure of the MCR-Hand II

Based on the design, development and test results of the MCR-Hand I [35], a linkage-and-tendon hybrid-driven anthropomorphic robotic hand, i.e. the MCR-Hand II is designed and presented in this paper. Figure 1 shows the mechanical design of the proposed robotic hand, it contains five fingers, a palm and an associated 3-DoF wrist. All the fingers, except for the middle finger, have four degrees of freedom and are actuated by three servo motors through linkage-and-

tendon hybrid transmission systems. The middle finger has three degrees of freedom actuated by two motors, it has no adduction/abduction degree of freedom. The palm is split into two sections along joint axis AB (as indicated in Fig. 1), providing flex for the ring and litter fingers. Joint AB is actuated by a servo motor SM-P/F through a four-bar linkage denoted as Linkage-P/F. The associated wrist has three degrees of freedom with the rotational motion (i.e. pronation and supination) directly actuated by servo motor SM-R. The adduction and abduction of the wrist are driven by servo motor SM-A/A through tendons denoted as Tendon-A/A, and the wrist flexion and extension is actuated by servo motor SM-F/E through a four-bar linkage denoted as Linkage-F/E. In this design, the robotic hand and wrist are driven by totally 17 four-bar 4R linkages and five tendons associated with return springs (elastic wires). This is a robotic hand with twenty degrees of freedom that is driven by fifteen actuators; and the attached wrist has three degrees of freedom driven by three actuators.

Dimension of the proposed robotic hand is in the size of an adult human hand such that lengths of the fingers are those of a human hand, and lengths of the phalanges in the hand are measured from a human hand as listed in Table 1. Based on the 3D printing technology, the aim of the proposed design is to achieve a robust and affordable lightweight anthropomorphic robotic hand with sufficient grasping power and human-like performance (such as in-hand manipulability). It is expected that the weight of the proposed hand will be less than 800g and the fingertip will be able to generate a force of over 3N.

Table 1. Lengths of phalanges in the MCR-Hand II (in mm)

Digit	Proximal	Middle	Distal	Total length
Index	46.4	33.2	25.2	104.8
Middle	54.4	38.2	28.2	120.8
Ring	51.4	38.2	25.2	114.8
Little	42.2	29.2	21.2	93.6
Thumb	Metacarpal	Proximal	Distal	
	44.2	39.7	21.2	105.1

2.2 Mechanical Design of the Fingers and Thumb

The detailed mechanical structures of the index, middle, ring and little fingers, and the thumb are illustrated in Fig. 2. For the finger, it has three joints including a DIP joint, a PIP joint, and a 2-DoF MCP joint denoted as MCP-1 and MCP-2 forming a universal joint. By mimicking the function of human hand [36–38], motion of the DIP joint is coupled with the PIP joint through a four-bar linkage denoted as 'DIP coupling linkage' in Fig. 2(a). Both the PIP and DIP joints are actuated by one servo motor denoted as Motor 1. In order to embed the motor in the proximal phalanx in the finger, another four-bar linkage denoted as 'PIP driving linkage' is used to transmit torque from Motor-1 to the PIP joint. Referring to [37] with additional calculation in Section 3.1, the motion range and transmission ratios between the DIP and PIP joints in the fingers are listed in Table 2. The joint angle ratio between the DIP and PIP joints for each of the finger is around 0.7 which is within the range revealed in [37].

Table 2. Motion range of the joints in the digits (in deg)

Joint	Index	Middle	Ring	Little	Thumb
MCP-1/CMC-1	0-105	0-94	0-109	0-104	0-98
MCP-2/CMC-2	7-30	-	7-20	7-30	0-120
PIP/MCP	0-107	0-107	0-107	0-107	0-103
DIP	0-75	0-78.6	0-78.6	0-76.2	0-85.2
Ratio(DIP/PIP)	0.7	0.73	0.73	0.73	0.71

Further, the MCP-1 joint is a tendon-driven joint, with the tendon indicated in Fig. 2(a) in the blue line, one end of the cable is fixed by an adjustable screw on the palmar side of the MCP-1 joint through a hole inside the finger, and the other end of the cable is connected to Motor 3 through the rails inside the palm. The tendon provides actuation for the flexion of the MCP joint, and the extension of MCP joint is achieved by the passive elastic wire, as indicated in green in Fig. 2(a). The elastic wire is made from 1mm crystal elastic stretch thread. Stiffness of the elastic wire is 0.1N/mm. There are two wires for each MCP-1 joint, hence the elastic coefficient of the wire should be 0.2N/mm. In addition, the adduction and abduction of the MCP joint, i.e. MCP-2 joint is actuated through a third four-bar linkage (denoted as MCP-2 driving linkage) by servo Motor 2. It

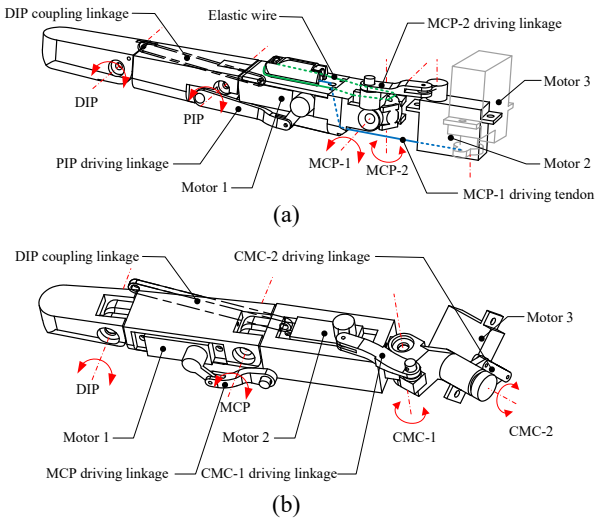

Fig. 2. (a) Detailed structure of the index, middle, ring and little fingers, and (b) detailed structure of the thumb.

should be pointed out that in this design, the middle finger has no MCP-2 joint due to the structure limitation. In addition, since the tendon does not pass through the rotation centre of the MCP-2 joint, when the fingers perform adduction and abduction, the tendon may be slack, and due to the tension of the elastic wire, the finger flexes slightly. This is common in tendon-driven based robotic hand design and can be solved by additional control strategy.

Moreover, as shown in Fig. 2(b), the thumb contains a DIP joint, a MCP joint and a 2-DoF CMC joint. The DIP joint is coupled with the MCP joint through a four-bar linkage denoted as DIP coupling linkage, and the MCP joint is driven by Motor 1 through a four-bar linkage denoted as MCP driving linkage. The CMC-1 joint is actuated by Motor 2 through another four-bar linkage denoted as CMC-1 driving linkage, and the CMC-2 joint is directly driven by Motor 3.

3 KINEMATICS OF THE HAND AND FINGERTIP FORCE ANALYSIS

Based on the mechanical design of the proposed MCR-Hand II, kinematics and force analysis of the hand are investigated in this section.

3.1 Kinematics of Linkages in the Hand

The proposed MCR-Hand II is a linkage-and-tendon hybrid driven anthropomorphic robotic hand. Linkages are used in the design of the digits, the splitting palm and the wrist. All these

linkages are four-bar 4R linkages as shown in Fig. 3. The four-bar 4R linkages are used in coupling the rotation between the DIP and PIP/MCP joints in the fingers/thumb, and driving the PIP and MCP-2 joints in the fingers, MCP, CMC-1 and CMC-2 joints in the thumb, the splitting joint in the palm, and the flexion-extension motion of the wrist. In all the 17 four-bar 4R linkages, the joint connected to a motor, or the driving joint in the coupling linkage, is labelled as A, the driven joint is labelled D, and the two joints on the coupler are labelled B and C, with B adjacent to A and C next to D. Lengths of links AD, AB, BC and CD are denoted as l_0, l_1, l_2, and l_3, respectively.

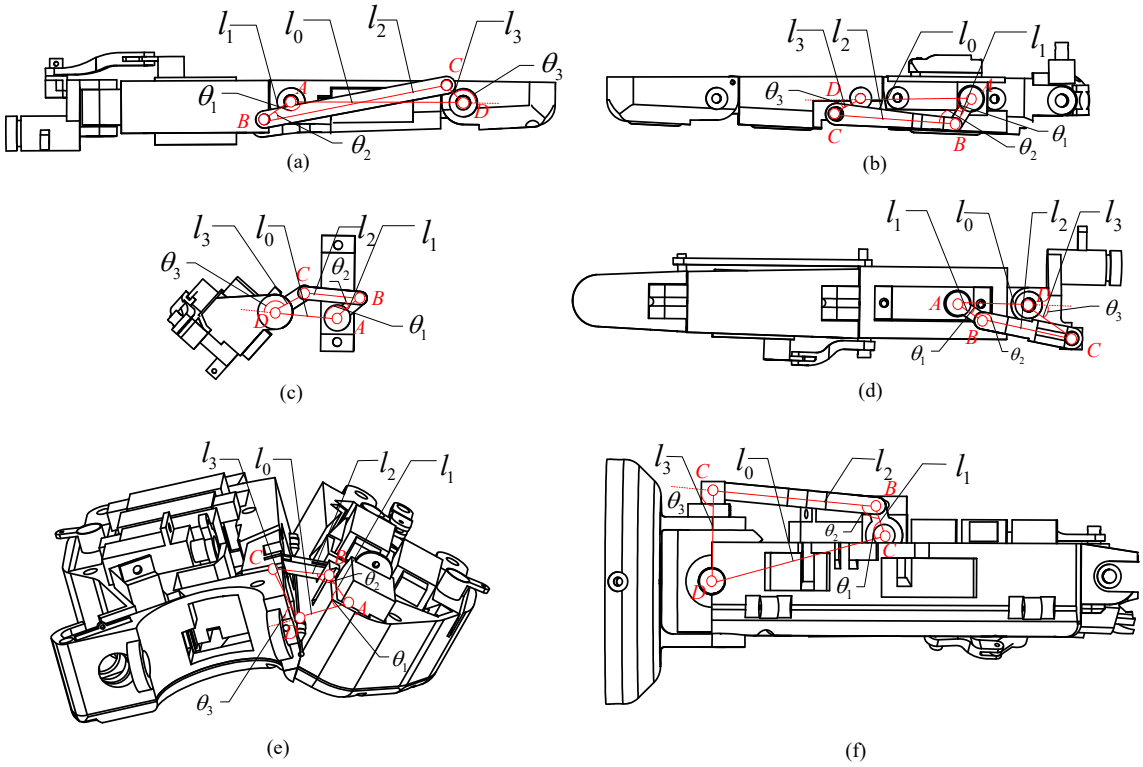

Fig. 3. The four-bar 4R linkages in the digits, the splitting palm and the wrist. (a) four-bar linkage coupling the DIP and PIP joints, (b) four-bar linkage driving the PIP joint, (c) four-bar linkage driving the CMC-2 joint, (d) four-bar linkage driving the MCP-2 joint, (e) four-bar linkage driving the palm splitting joint, and (f) four-bar linkage driving the wrist flexion/extension.

Let the driving joint angle associated with joint A be θ_1 and the driven joint angle at joint D be θ_3, based on the classical formulation for a four-bar-4R linkage, the relation between θ_1 and θ_3 can

be obtained as

$$\theta_3 = \arctan\left(\frac{B}{A}\right) \pm \arccos\left(\frac{C}{\sqrt{A^2+B^2}}\right) \tag{1}$$

with $A = 2l_1l_3\cos\theta_1 - 2l_0l_3$, $B = 2l_1l_3\sin\theta_1$, and $C = l_0^2 + l_1^2 + l_3^2 - 2l_0l_1\cos\theta_1$. In Eq. (1), due to the rotation limitation of the servo motors, only the positive solution is valid. Once the angle θ_3 is obtained, the coupler angle θ_2 can be derived as

$$\theta_2 = \arctan\left(\frac{l_3\sin\theta_3 - l_1\sin\theta_1}{l_0 + l_3\cos\theta_3 - l_1\cos\theta_1}\right) \tag{2}$$

By carefully assigning the link lengths of the four-bar linkages (see Appendix A) according to the sizes of the phalanges listed in Table 1, and then using Eqs. (1) and (2) the rotation ranges of the finger joints are obtained and listed in Table 2.

Additionally, the rotation range of the palm splitting joint AB is 0° - 55.5° driven by a servo motor of rotation range 0° - 44.9°.

3.2 Kinematics and Workspace of the MCR-Hand II

As shown in Fig. 4, in order to study the kinematics of the hand, a reference coordinate system is established at point O and by following the D-H convention [39], body-attached frames are assigned to each of the joints and tips of the fingers and thumb.

Then based on the D-H parameters (see Appendix B), postures of the tips of the fingers and thumb can be obtained as

$$\mathbf{T}_n^0 = \mathbf{T}_1^0\mathbf{T}_2^1\ldots\mathbf{T}_n^{n-1} \tag{3}$$

Where matrix $\mathbf{T}_j^i$ is the homogeneous matrix giving both position and orientation of frame j

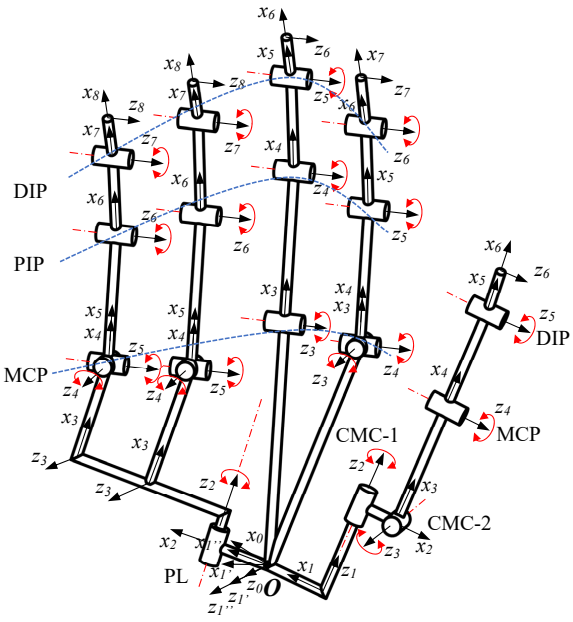

Fig. 4. Geometry and coordinate systems in the hand.

with respect to frame i. For the thumb, $n = 6$; for the index finger, $n = 5$; for the middle finger, $n = 4$; and for the ring and litter fingers, $n = 7$.

Using the kinematic results from Eqs. (1) and (2), and Table 2 for identifying the joint angles in the digits, workspace of the whole hand is computed and generated as shown in Fig. 5. Workspace of the thumb is in purple, the index finger in black, the middle finger in red, the ring finger in blue, and the little finger in green. Due to the lack of the MCP-2 joint, workspace of the middle finger lies in a plane. It is noted that due to the introduction of the splitting palm through joint AB (see Fig. 1), workspace of the ring and little fingers is larger than that of the previous version of the proposed robotic hand (i.e. MCR-Hand I as discussed in [35]) with a rigid palm: for the ring finger, workspace of the splitting palm is 701.5mm^3, and of the rigid palm is 190.8mm^3; about 367.6 % larger. In addition, workspace of the little finger for the MCR-Hand II is 420.6% larger than that of MCR-Hand I. Further, through the splitting palm, thumb opposability [40] is significantly improved due to the increase of common workspace between the thumb of the ring and little fingers; as demonstrated in the Kapandji score tests in Section 5.

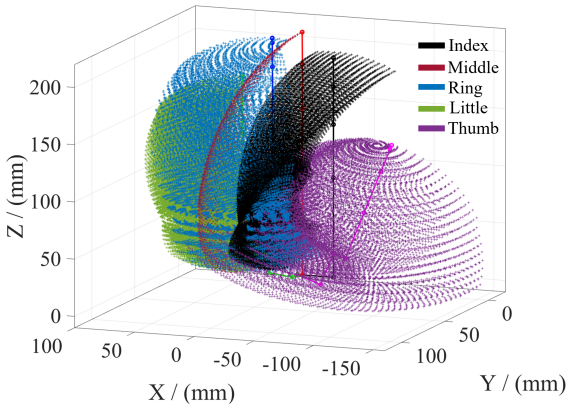

Fig. 5. Workspace of the MCR-II hand, the thumb is in purple, the index finger in black, the middle finger in red, the ring finger in blue, and the little finger in green.

3.3 Fingertip Force Analysis

In robotic hand design, in order to install more actuators inside the robotic hand to achieve hand dexterity without increasing its size, it is not easy to use actuators with a larger output torque and high speed due to its limited size. In the proposed robotic hand design, a trade-off is made between dexterity and fingertip force. However, fingertip force is an important index in quantifying the performance of a robotic hand; it determines the quality of objects the robotic hand can hold stably and what kind of operations it can perform. Therefore, it is important to ensure that the MCR-Hand II has sufficient fingertip force.

3.3.1 Force from the MCP-1 joint

Figures 6(a), (b) and (c) show the structure of the MCP-1 joint in the finger, where $MS-MN-NJ$ represents the control wire. When the rudder of the servo (denoted by OS as shown in Fig. 6(b)) rotates by an angle α, the control wire will be pulled from MS_1 to MS_2, wherein MS_1 is the original position of the rudder. Let μ be the pressure angle as indicated in Fig. 6(c), referring to the figure, the tension applied to the control wire from the rudder is

$$F = F_0/\cos\mu \tag{4}$$

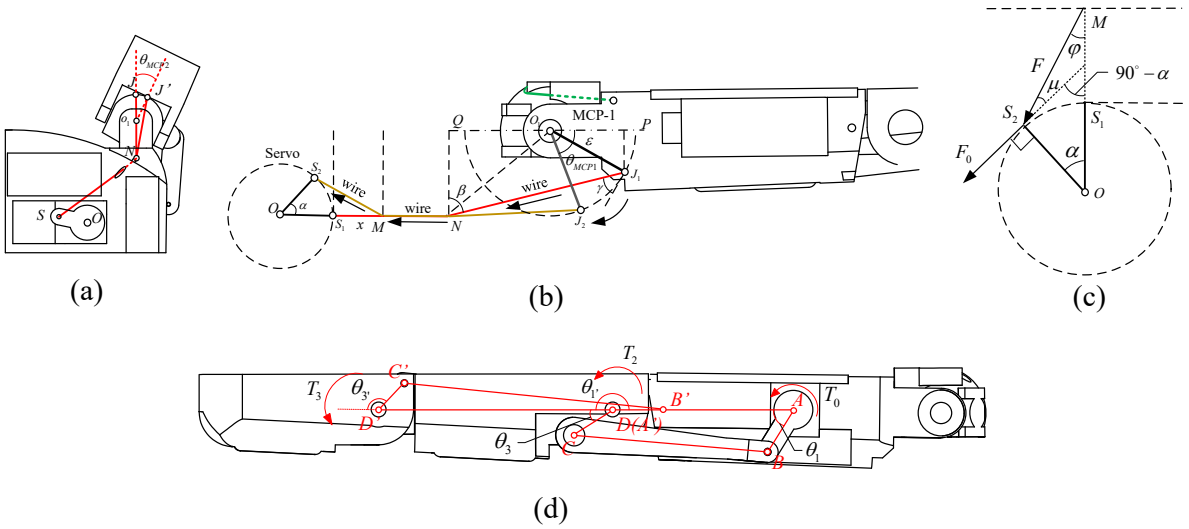

Fig. 6. Structure and force transmission in the MCP-1 joint and the PIP and DIP joints. (a) Tendon path, (b) Force transmission diagram, (c) relationship between F and F_0, (d) Torque relationship in the PIP and DIP joints.

in which F_0 represents the output force from the servo. μ stands for the pressure angle of the input, and can be derived from Fig. 6(c) as

$$\mu = \pi/2 - \alpha - \varphi \tag{5}$$

where φ is the angle of $\angle OMS_2$ which can be related to $\overline{MS_1}$ as $\varphi = \arccos\left(\left(\left(\overline{MS_1 + OS_1}\right)^2 + \overline{MS_2^2} - \overline{OS_2^2}\right)/2\overline{M}\right.$

Subsequently, referring to Fig. 6(b), the tension applied to the MCP-1 joint is

$$F_{out} = F\cos\gamma \tag{6}$$

where γ is the pressure angle of the output at the MCP-1 joint.

Hence from Fig. 6(b), the output torque at the MCP-1 joint can be expressed as

$$T_{out} = F_{out} \cdot \overline{O_1 J} = F_0 \cos\gamma \cdot \overline{O_1 J}/\cos\mu \tag{7}$$

It is noted that μ is related to the length of $\overline{MS_1}$ as the angle φ is related to $\overline{MS_1}$, which is different in each finger.

When the MCP-1 joint rotates, the elastic wire which controls the joint's return to its original position will generate a resistance torque T_r as

$$T_r = F_r \cdot \overline{O_1 J} = \left(k \cdot \theta_{MCP-1} \cdot \overline{O_1 J} + F_{r0} \cdot \overline{O_1 J}\right) \tag{8}$$

where F_{r0} represents the initial resistance from the elastic wire, k is the elastic coefficient of the wire, and θ_{MCP-1} is the angle change of the MCP-1 joint.

Hence, considering that with the same fingertip force, the MCP-1 joint needs to sustain the largest torque, the output force at the fingertip can be expressed as

$$F_{f1} = \frac{(T_{out} - T_r - T_f)}{L_{f1}} \tag{9}$$

where F_{f1} denotes the force at the fingertip, direction of the force is perpendicular to the line connecting O_1 and the fingertip; having an angle with the plane of fingertip ventral surface. T_f is the torque generated by friction. L_{f1} is the distance from the fingertip to the centre of the MCP joint, it varies according to the finger position and configuration.

3.3.2 Force for the DIP and PIP joints

Both the DIP and PIP joints are driven by one servo through two sets of four-bar 4R linkages. Based on the kinematic analysis in Section 3.1 and referring to Fig. 6(d), by neglecting fiction in the joints, the torque at the PIP joint can be expressed as

$$T_2 = \frac{l_3 \sin(\theta_3 - \theta_2)}{l_1 \sin(\theta_1 - \theta_2)} T_0 \tag{10}$$

where, l_3, l_1, θ_1, θ_2 and θ_3 are parameters and joint angles of the four-bar 4R mechanism for actuating the PIP joint. T_0 is the input torque of the servo, and T_2 stands for the output torque at the PIP joint.

Subsequently, since the DIP joint is coupled with the PIP joint through another four-bar 4R mechanism, the output torque at the DIP joint is

$$T_3 = \frac{l_{2'} \sin(\theta_{3'} - \theta_{2'})}{l_{1'} \sin(\theta_{1'} - \theta_{3'})} T_2 \tag{11}$$

with $l_{3'}$, $l_{1'}$, $\theta_{2'}$ and $\theta_{3'}$ being parameters and joint angles of the four-bar 4R mechanism for coupling the DIP joint. $\theta_{1'} = \theta_3 + \pi - \theta_{30}$ with θ_{30} being the initial angle of θ_3, T_3 represents the output torque at the DIP joint.

Hence the fingertip force from the DIP and PIP joints can be obtained from Eqs. (10) and (11) as

$$F_{f2} = \frac{T_2}{L_{f2}} \text{ and } F_{f3} = \frac{T_3}{L_{f3}} \tag{12}$$

where L_{f2} and L_{f3} are the distances for the fingertip to the centres of the PIP and DIP joints, respectively.

Given the normal input servo torques, 0.35Nm at the MCP-1 joint and 0.08Nm at the PIP joint, using Eqs. (9) and (12), through computer simulation, fingertip force generated from the MCP-1, PIP and DIP joints can be obtained as illustrated in Fig. 7.

Figure 7 shows the relation between the joint angles and the corresponding output forces on the fingertip. It can be seen that each joint in the fingers can generate a fingertip force of approximately 2N.

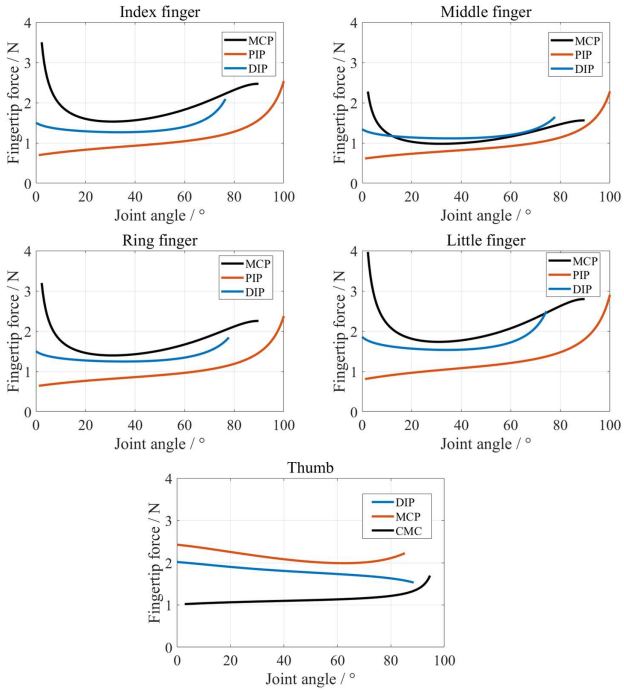

Fig. 7. The relation between joint angles and output forces on fingertips of the fingers and thumb.

4 MECHATRONIC SYSTEM INTEGRATION AND CONTROL

4.1 Actuation

All of the actuators are under economic consideration. In MCR-Hand II, the actuators for the PIP and DIP joints of the fingers are mounted inside the proximal phalanges. Hence, the size of the servo should be small enough. Considering this, the commercial compact servo, i.e. Hitec HS-5035HD was chosen as the actuators for the PIP/DIP joints. The servos that actuate the MCP-2 joint of the finger and the CMC, MCP and DIP joints of the thumb are located inside the palm, and thus the HS-5035HD servo is selected to drive these joints.

Further, since the MCP-1 joint in the finger is one of the most important joints that needs high torque for generating great grasping force, considering that extension of the MCP-1 joint is achieved by elastic wire, torque of the servo actuating the MCP-1 joint should be large enough to pull the elastic wire and to generate an adequate torque for grasping tasks. In order to meet such a requirement, the servo, i.e. MKS, DS450 was selected and used to drive the MCP-1 joint. The same servo is used for three joints in the wrist due to the high torque demanded. In addition, for the splitting joint AB, the servo Futaba S3108M was used according to the torque required. In

total, there are ten HS-5035DH servos, seven DS450 servos, and one S3108M servo used in the development of MCR-Hand II.

4.2 Electronics and Control

The MCR-Hand II is designed to be equipped with embedded electronics for low-level control of the hand. In order to keep the size of the robotic hand approximate to the size of a human hand, servo controller Maestros™ was used to control all the servos. This is a controller with eighteen multiple function channels which allow PWM (pulse-width modulation) output and analog input; its precise and high-resolution servo pulses make the controller well fit high-performance robots. The built-in speed and acceleration controller makes it easy to achieve smooth movements.

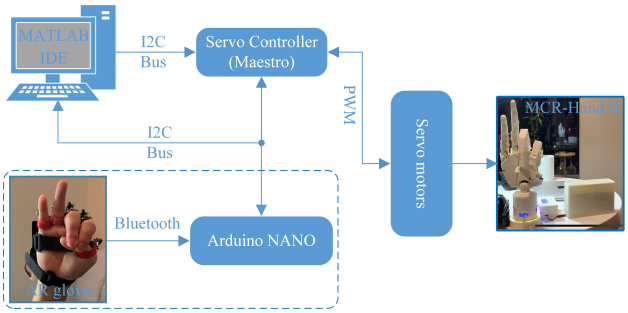

Fig. 8. Sevro-based micro-controller system integration.

Figure 8 shows the micro-controller system of the MCR-Hand II. There are two control schemes, i.e. one through direct PC control and the other through AR glove control. For the PC control, the servo controller (Maestros) receives digital signals including joint angles, and angular speeds and accelerations from the software interface on the PC and sends PWM signals to the servo motors leading to the motion of the robotic hand. The current positions in the servos are fed back to the software interface on the PC through the controllers. During the lack of sensory feedback, grasping must be predefined and pre-programmed.

In the AR glove control, a commercial AR glove is used to achieve master-slave control of the robotic hand. The AR glove provides the positions of the MCP-1 joint (MCP joint for the thumb) through five potentiometers. The position data are transmitted to the Arduino nano via Bluetooth, which computes desired PWM signals for the micro controller Meastro. However, in this control

scheme, only joint angles of the MCP-1 joints are obtained as inputs from the AR glove, the angles of PIP joints need to be predefined according to a specified grasping task.

5 PROTOTYPE, EMPIRICAL STUDY AND EVALUATION

All the parts of MCR-Hand II except for the electronic components and screws, are printed by dual extrusion 3D printer Ultimaker 3^{TM}. The dual extrusion allows water-soluble support material to be used to create complex mechanical parts, which results in smooth and professional finish. Several materials are applied to print the prototype of the MCR-Hand II, including PLA, TPU 95A (soft material at fingertip), and Ultimaker Breakaway (print the supports).

The MCR-Hand II is characterized by the linkage-tendon hybrid driven scheme. Palm of the MCR-Hand II is designed to accommodate the 17 servos for driving the splitting palm and digits without interference. 51 wires including tendons, elastic wires and electronic wires are handily arranged in the digits, palm. Controllers and Arduino chips are all located inside a short section of forearm below the wrist.

Cost for the prototype of MCR-Hand II developed in this paper is approximate $500 (see Appendix D the detailed costs for all the components [41]). Comparing with the commercially available robotic hands listed in Table 3, it can be found that the MCR-Hand II is an affordable light-weight robotic hand which can provide capabilities for manipulations that require the closest approximation of the human hand. It should be noted that in the table, hand size is the ratio between the size of a robotic hand and that of an adult human hand.

Table 3. Some commercial robotic hands and the MCR-Hand II

Name	DoF	Actuator Number	Weight (kg)	Size	Payload (kg)	Fingertip force (N)	Price U
Shadow Hand	24	20	4.3	1.2	4	-	$> 60,0$
Hand-Lite	16	13	2.4	1.2	4	10	$> 10,0$
DLR-HIT Hand II	15	10	1.5	1.0	-	10	$> 14,0$
Schunk Hand	20	9	1.3	1.0	-	5	$54,00$
MCR-Hand II	20	18	0.8	1.2	1.8	3	< 500

5.1 Fingertip Force Evaluation

To evaluate the fingertip force [40, 42–44] generated by each finger, the robotic hand is placed on the table. An electronic scale with a long cube is placed in front of the robotic hand as shown in Fig. 9. The surface of the cube is at the distance and height that the fingertips can touch. The robotic hand is fixed on the table so that it remains stable during the experiment. A positioner is used to control the robotic finger to flex, touch and press the surface of the cube. Reading from the electronic scale is the fingertip force at the current position. The thumb adopts the method of holding the palm of the robotic hand by hand and then use the positioner to control the thumb fingertip to directly press the surface of the electronic scale. It should be noted that the electronic scale is cleared after placing the cube. It is found through experiments that when a stable voltage of 6V is provided, the robotic hand can generate peak fingertip forces of 3.8N, 2.8N, 3.2N, 3.1N, and 4.1N for the index, middle, ring, little finger and thumb, respectively. These results are consistent with the theoretical results obtained in Section 3.3.

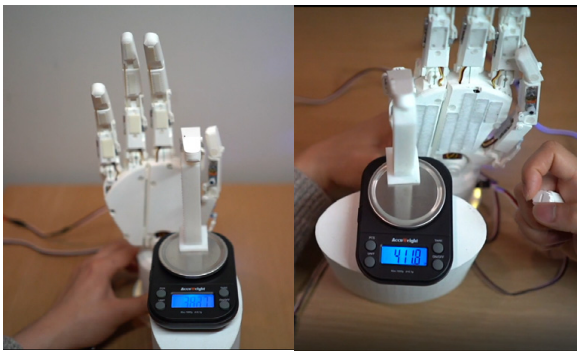

Fig. 9. Electronic scale based fingertip force evaluation.

Subsequently, using the proposed prototype, three conventional tests are carried out so as to check the performance of the MCR-Hand II.

5.2 Kapandji Score Test

Thumb opposition is important for hand grasping and the Kapandji score [45] is a clinical tool for evaluating the opposability of the thumb. Based on the part of the hand that the thumb fingertip

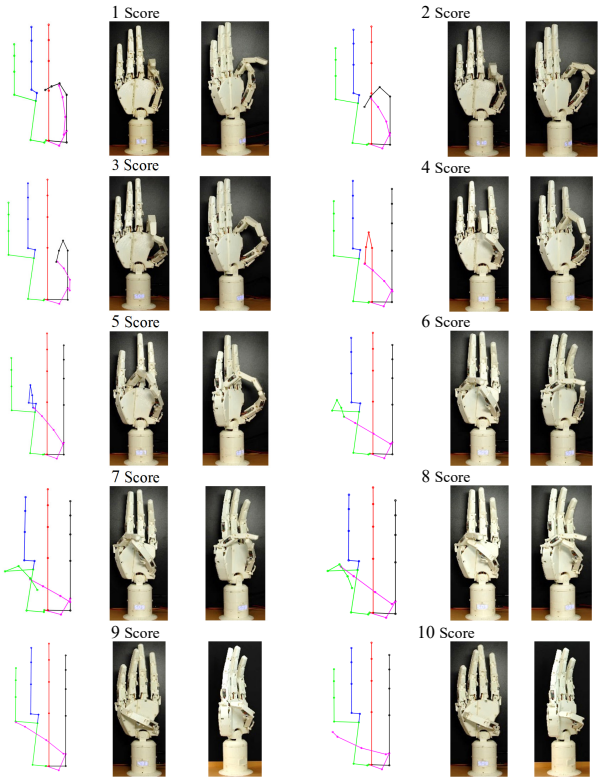

Fig. 10. Kapandji Score Test for thumb opposition.

is able to touch, thumb opposition is scored from 0 to 10 with a score of 0 indicating no opposability and a score 10 implying maximal opposability. Figure 10 shows the thumb opposition tests both in the kinematic simulation and prototype implementation, it indicates that the proposed hand is capable of scoring thumb opposability in the range of 0 to 10; the introduction of the palm flex by the splitting joint helps enhance the manipulability of the proposed robotic hand.

5.3 Cutkosky Taxonomy

The above Kapandji score test results imply that the majority of common hand gestures can be performed by the MCR-Hand II. Since the main application of robotic hands is for work in factories to replace human hands, in this section the Cutkosky Taxonomy [46] is used to evaluate the performance of the proposed robotic hands. There are 16 different types of grasping poses in the Cutkosky taxonomy, which are divided into power grasping and precision grasping. By using the MCR-Hand II, a static evaluation was conducted to determine whether the hand could complete the grasping poses listed in the Cutkosky taxonomy and the results are illustrated in Fig.

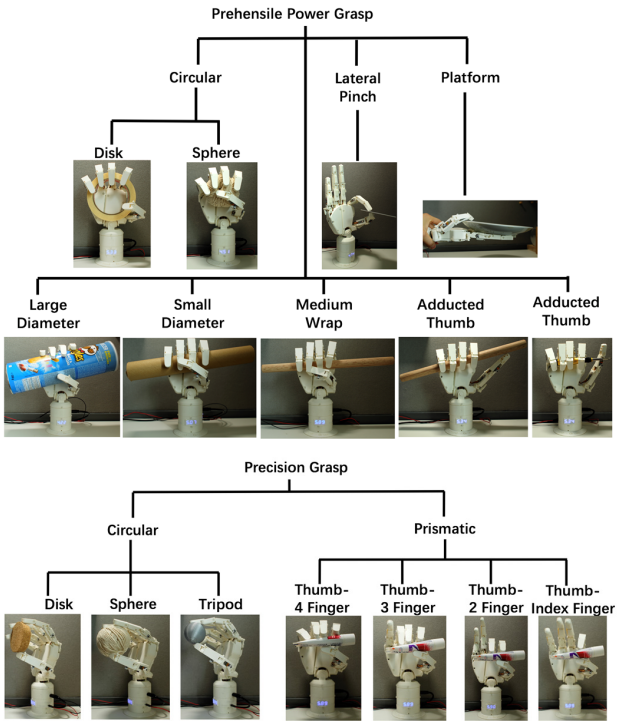

Fig. 11. Grasping poses performed by the MCR-Hand II according to Cutkosky taxonomy.

11. It should be noted that due to the cost-effective design, the servos chosen are under economic consideration and thus the output force from the MCR-Hand II is not as strong as that of a human hand. Hence, in the Cutkosky taxonomy test, light objects were chosen to test the prototype of MCR-Hand II.

5.4 Kamakura Taxonomy

Further, the MCR-Hand II might also be used as a service robot or prosthesis for individuals in daily life. Therefore, the Kamakura taxonomy test [42] is applied to investigate the performance of the MCR-Hand II in daily life activities. Kamakura has advocated the grip classification based on grip in daily life. The meaning of each abbreviation is shown in Appendix C. Items are chosen to meet the requirement of the test, and are a kitchen knife (89g), wooden stick (120g), glass bowl (204g), spoon (48g), chopsticks, medicine bottle (50g), ball (30g), scissors (63g), pin, paper and brush.

Experimental results of Kamakura taxonomy test using MCR-Hand II is shown in Fig. 12. It should be pointed out that the MCR-Hand II failed to complete the T-I type (tripod-grasp) grasp due

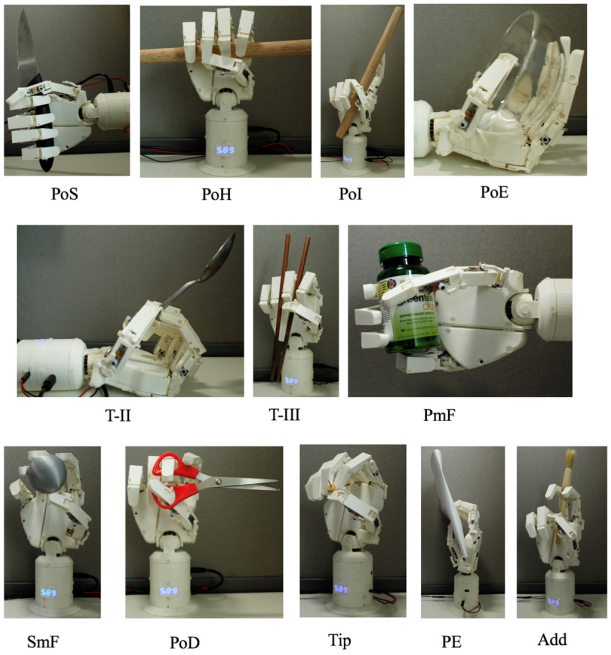

Fig. 12. Kamakura Taxonomy performed by the MCR-Hand II.

to insufficient fingertip friction. As a result, it is evident that almost all the grasp types are sufficiently well-holding, however, the friction of the fingertips may need to be increased. Furthermore, there may also be a need to change the shape of the fingertips in the current model to mimic the flexible structure of the human fingertips, which have a soft spherical curved surface. In addition, the recent proposed taxonomy, i.e. the GRASP taxonomy [47] can be considered in our future investigation for grasping measurement.

5.5 Object Manipulation

Other than grasping objects, robotic hands are required to complete manipulation tasks for the high demand in industry and service use. In this research, the dexterity of the MCR-Hand was experimentally demonstrated by completing a motion group often use in daily life: rotating and opening a bottle cap. The test involved precision grasp a cylindrical object (cap) and rotate with finger abduction and thumb flexion. Figure 13 shows the process of the manipulation test. In the test, the MCR-Hand II was fixed on the right arm of a ABB YuMi® robot. The bottle with a screwed cap was fixed on the left arm. The positions of the robotic hand and the bottle were set in advance by the YuMi robot. During the test, the robotic arm was not involved. In Fig. 13, the diagram below

the action snapshot shows the top view of the index finger and thumb fingertips. Among them, the brown circle indicates the cap, the grey dots indicate the previous positions of the fingertips of the finger and the thumb, the black dots indicate the end positions of current motion. Arrows indicate the direction of fingertip movement.

In this manipulation process, we first keep the fingertip of the index finger and thumb away from the cap (see Fig. 13(a)). Then, the index finger flex and the thumb adduct until in contact with the cap surface and generate pressure (see Fig. 13(b)). Rotate the cap by abducting the index finger and flexing the thumb; after the cap rotates at a certain angle, the index finger extent and thumb abduct, so that the index finger and thumb will not touch the cap surface during the next motion. Next, the index finger adduct and thumb extended to return its initial position. Repeat the above steps until the cap unscrewed (see Figs. 13(c) to (g)). Ultimately, the hand lifts the cap with wrist extension (see Fig. 13(h)).

Through the above operation, the bottle cap was successfully unscrewed and lifted.The manipulation test presented in this section effectively demonstrated the remarkable dexterity of the MCR-Hand II. The experimental results show that the adduction/abduction of finger and thumb is extremely important in manipulability of a robotic hand.

6 CONCLUSIONS

In this paper, a low-case anthropomorphic robotic hand, i.e. MCR-Hand II was for the first time introduced. The proposed robotic hand uses a new transmission system that combines both tendon-driven and linkage-driven systems. Using such transmission system and economic servo motors, a compact structure of designing robotic hand to imitate all DOFs and function of a human hand was achieved. In addition, the proposed MCR-Hand II has a split palm and a 3-DOF wrist which greatly enhance workspace, dexterity and performance of the hand. Mechanical design, kinematics and force analysis of the proposed hand were presented with simulation results. Further, prototype of the proposed hand was developed integrated with low-level control systems. Three widely accepted test were applied to evaluate the performance of MCR-Hand II. The Kapandji score was used to classify the opposability of the thumb and results indicate that the MCR-

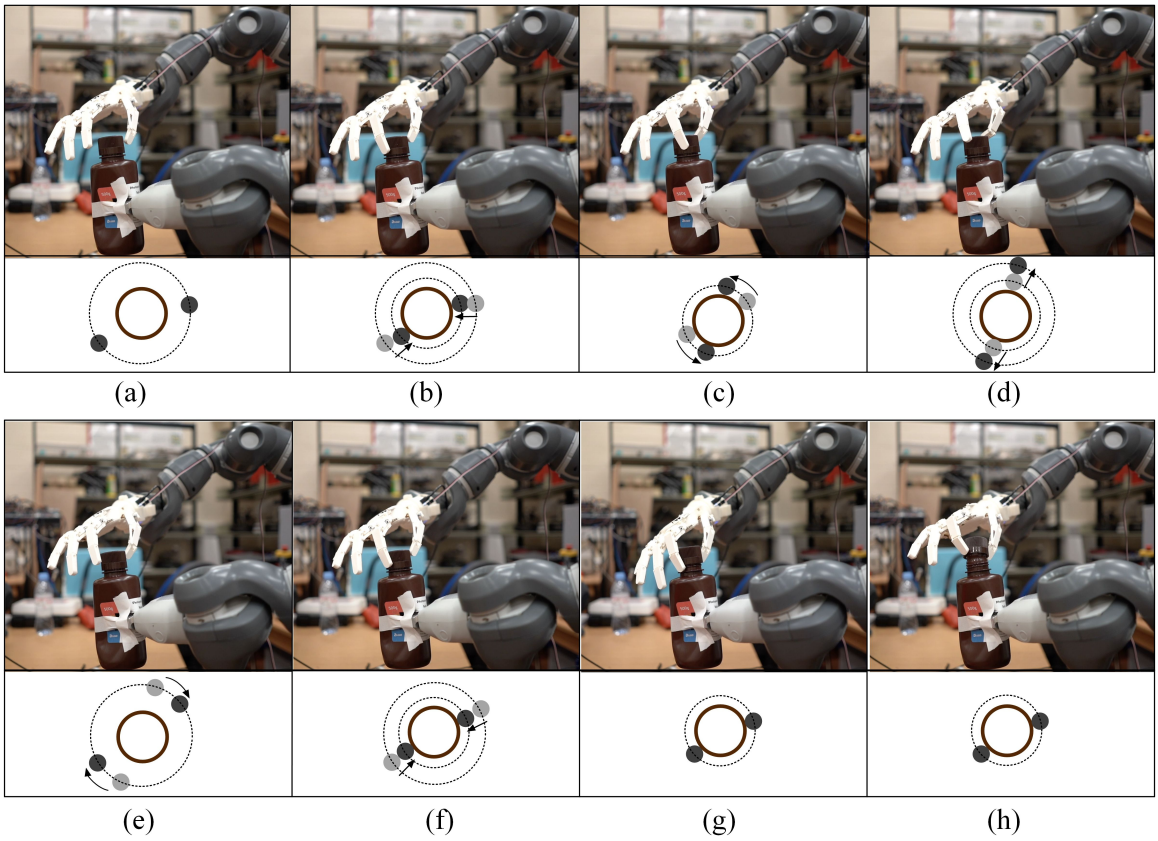

Fig. 13. Dexterous manipulation test with YuMi robot: unscrew and lift a cap. The diagram shows the top view of the index finger and thumb fingertips. The brown circle indicates the cap, the grey dots indicate the previous positions of the fingertips, the black dots indicate the end positions of current motion. Arrows indicate the direction of fingertip movement.

Hand II could reach all the test points. The Cutkosky taxonomy was used to test the grasping motion of robotic hands under factory condition. Results show that the MCR-Hand II was successfully able to perform all grasping poses including power grasp and precision grasp. In addition, the Kamakura taxonomy was applied to evaluate the grasping ability of the proposed hand in daily life object manipulation. Object manipulation was also demonstrated through the bottle cap unscrew and lift operation. Results demonstrate that MCR-Hand II was able to perform almost all poses successfully, however, the fingertip friction may need to be increased in the future.

Hence, this paper has introduced the tendon-and-linkage hybrid-driven system in the design of compact and affordable robotic hand that can be used for practical grasping and manipulation tasks in both industrial and domestic environment.

ACKNOWLEDGEMENTS

This work is partly supported by the projects of National Natural Science Foundation of China under Grant No. 91948302 and No. 91848204, and the project of National Key R&D Program of China under No. 2018YFC2001300.

REFERENCES

[1] Tomovic, R., and Boni, G., 1962. "An adaptive artificial hand". *IRE Transactions on Automatic Control,* **7**(3), pp. 3–10.

[2] Piazza, C., Grioli, G., Catalano, M. G., and Bicchi, A., 2019. "A century of robotic hands". *Annual Review of Control, Robotics, and Autonomous Systems,* **2**(1), pp. 1–32.

[3] Tai, K., El-Sayed, A. R., Shahriari, M., Biglarbegian, M., and Mahmud, S., 2016. "State of the art robotic grippers and applications". *Robotics,* **5**(2), p. 11.

[4] Childress, D. S., 1985. "Historical aspects of powered limb prosthese". *Clinical Proesthetics & Orthotics,* **9**(1), pp. 2–13.

[5] Okada, T., 1982. "Computer control of multjointed finger system for precise object-handing". *IEEE Transactions oon Systems, Man and Cybernetics,* **12**(3), pp. 289–299.

[6] Jacobsen, S., Iversen, E., Knutti, D., Johnson, R., and Biggers, K., 1986. "Design of the Utah/M.I.T. dextrous hand". In 1986 IEEE International Conference on Robotics and Automation, Vol. 3, pp. 1520–1532.

[7] Nakano, Y., Fujie, M., and Hosada, Y., 1984. "Hitachi's robot hand". *Robotics Age,* **6**(7), pp. 18–20.

[8] Caffaz, A., and Cannata, G., 1998. "The design and development of the DIST-hand dextrous gripper". In 1998 IEEE International Conference On Robotics And Automation, pp. 2075–2080.

[9] Lovchik, C. S., and Diftler, M. A., 1999. "The Robonaut hand: a dexterous robot hand for space". In Proceedings 1999 IEEE International Conference on Robotics and Automation, Vol. 2, pp. 1050–4729.

[10] Bridgwater, L. B., Ihrke, C. A., Diftler, M. A., Abdallah, M. E., Radford, N. A., Rogers, J. M.,

Yayathi, S., Askew, R. S., and Linn, D. M., 2012. "The Robonaut 2 hand - designed to do work with tools". In 2012 IEEE International Conference on Robotics and Automation, pp. 3425–3430.

[11] Liu, H., Butterfass, J., Knoch, S., Meusel, P., and Hirzinger, G., 1999. "A new control strategy for DLR's multisensory articulated hand". *IEEE Control Systems Magazine,* **19**(2), pp. 47–54.

[12] Butterfass, J., Grebenstein, M., Liu, H., and Hirzinger, G., 2001. "DLR-hand II: Next generation of a dextrous robot hand". In Proceedings of the 2001 IEEE International Conference on Robotics & Automation.

[13] Friedl, W., Hoppner, H., Petit, F., and Hirzinger, G., 2011. "Wrist and forearm rotation of the DLR hand arm system: Mechanical design, shape analysis and experimental validation". In 2011 IEEEIRSJ International Conference on Intelligent Robots and Systems, pp. 1836–1842.

[14] Dai, J. S., Wang, D. L., and Cui, L., 2009. "Orientation and workspace analysis of the multifingered metamorphic hand - Metahand". *IEEE Transactions on Robotics,* **25**(4), pp. 942–947.

[15] Wei, G., Dai, J. S., Wang, S., and Luo, H., 2011. "Kinematic analysis and prototype of a metamorphic anthropomorphic hand with a reconfigurable palm". *International Journal of Humanoid Robotics,* **8**(3), pp. 459–479.

[16] Emmanouil, E., Wei, G., and Dai, J. S., 2016. "Spherical trigonometry-based kinematics for controlling a dexterous robotic hand with an articulated palm". *Robotica,* **34**, pp. 2788–2805.

[17] Cui, L., and Dai, J., 2011. "Posture, workspace, and manipulability of the metamorphic multifingered hand with an articulated palm". *Journal of Mechanisms and Robotics, Trans. ASME,* **3**(2), p. 021001.

[18] Laliberte, T., Birglen, L., and Gosselin, C. M., 2002. "Underactuation in robotic grasping hands". *Machine Intelligence & Robotic Control,* **4**(3), pp. 1–11.

[19] Catalano, M., Grioli, G., Farnioli, E., Serio, A., Piazza, C., and Bicchi, A., 2014. "Adaptive synergies for the design and control of the pisa/iit softhand". *The International Journal of Robotics Research,* **33**(5), pp. 768–782.

[20] Deimel, R., and Brock, O., 2016. "A novel type of compliant and underactuated robotic hand for dexterous grasping". *International Journal of Robotics Research,* **35**, pp. 161–185.

[21] Terryn, S., Brancart, J., Lefeber, D., Van Assche, G., and Vanderborght, B., 2017. "Self-healing soft pneumatic robots". *Science Robotics,* **2**, p. eaan4268.

[22] Nassour, J., Ghadiya, V., Hugel, V., and Hamker, F., 2018. "Design of new sensory soft hand: combining airpump actuation with superimposed curvature and pressure sensors". In 2018 IEEE International Conference on Soft Robotics (RoboSoft), pp. 164–169.

[23] Salisbury, J. K., and Craig, J. J., 1982. "Articulated hands: force control and kinematic issue". *The International Journal of Robotics Research,* **1**(1), pp. 4–17.

[24] Deshpande, A. D., Xu, Z., Weghe, M. J. V., Brown, B. H., Ko, J., Chang, L. Y., Wilkinson, D. D., Bidic, S. M., and Matsuoka, Y., 2013. "Mechanisms of the anatomically correct testbed hand". *IEEE/ASME Transactions on Mechatronics,* **18**(1), pp. 238–250.

[25] Palli, G., Melchiorri, C., Vassura, G., Scarcia, U., Moriello, L., Berselli, G., Cavallo, A., Maria, G. D., Natale, C., Pirozzi, S., May, C., Ficuciello, F., and Siciliano, B., 2014. "The DEXMART hand: Mechatronic design and experimental evaluation of synergy-based control for human-like grasping". *The International Journal of Robotics Research,* **33**(5), pp. 799–824.

[26] Mouri, T., Kawasaki, H., Yoshikawa, K., Takai, J., and Ito, S., 2002. "Anthropomorphic robot hand: Gifu hand III". In Proceedings of the International Conference ICCAS, pp. 1288–1293.

[27] Ueda, J., Ishida, Y., Kondo, M., and Ogasawara, T., 2005. "Development of the NAIST-hand with vision-based tactile fingertip sensor". In Proceedings of the 2005 IEEE International Conference on Robotics and Automation, pp. 2332–2337.

[28] Cerruti, G., Chablat, D., Gouaillier, D., and Sakka, S., 2016. "ALPHA: A hybrid self-adaptable hand for a social humanoid robot". In 2016 IEEE/RSJ International Conference on Intelligent Robots and Systems (IROS), pp. 900–906.

[29] Zhang, Z., Han, T., Pan, J., and Wang, Z., 2018. "CATCH-919 hand: Design of a 9-actuator 19-dof anthropomorphic robotic hand". *arXiv,* **1809.04290**.

[30] Carrozza, M. C., Cappiello, G., Stellin, G., Zaccone, F., Vecchi, F., Micera, S., and Dario, P., 2005. "A cosmetic prosthetic hand with tendon driven under-actuated mechanism and compliant joints: Ongoing research and preliminary results". In Proceedings of the 2005 IEEE International Conference on Robotics and Automation, pp. 2661–2666.

[31] Controzzi, M., Clemente, F., Barone, D., Ghionzoli, A., and Cipriani, C., 2017. "The SSSA-MyHand: A dexterous lightweight myoelectric hand prosthesis". *IEEE Transactions on Neural Systems and Rehabilitation Engineering,* **25**(5), pp. 459–468.

[32] Scharff, R., Doubrovski, E., Poelman, W., Jonker, P., Wang, C., and Geraedts, J., 2016. "Towards behavior design of a 3d-printed soft robotic hand". In *Soft Robotics: Trends, Applications and Challenges*, C. Laschi, J. Rossiter, F. Iida, M. Cianchetti, and L. Margheri, eds., Vol. 17 of *Biosystems & Biorobotics*. Springer.

[33] Ma, R., and Dollar, A., 2017. "Yale OpenHand project: Optimizing open-source hand designs for ease of fabrication and adoption". *IEEE Robotics & Automation Magazine,* **24**(1), pp. 32–40.

[34] Kontoudis, G. P., Liarokapis, M. V., Zisimatos, A. G., Mavrogiannis, C. I., and Kyriakopoulos, K. J., 2015. "Open-source, anthropomorphic, underactuated robot hands with a selectively lockable differential mechanism: Towards affordable prostheses". In 2015 IEEE/RSJ International Conference on Intelligent Robots and Systems (IROS), p. 5.

[35] Yang, H., Wei, G., and Ren, L., 2019. "Design and development of a linkage-tendon hybrid driven anthropomorphic robotic hand". In International Conference on Intelligent Robotics and Applications (ICIRA 2019), pp. 117–128.

[36] Chao, E. Y. S., An, K.-N., Cooney III, W. P., and Linscheid, R. L., 1989. *Biomechanics of the Hand*. World Scientific, Farrer Road, Singapore.

[37] HAHN, P., KRIMMER, H., HRADETZKY, A., and LANZ, U., 1995. "Quantitative analysis of the linkage between the interphalangeal joints of the index finger: An in vivo study". *The Journal of Hand Surgery,* **20**(5), pp. 696–699.

[38] Birglen, L., 2011. "The kinematic preshaping of triggered self-adaptive linkage-driven robotic fingers". *Mechanical Sciences,* **2**(1), pp. 41–49.

[39] Lipkin, H., 2005. "A note on Denavit-Hartenberg notation in robotics". In Proceedings of International Design Engineering Technical Conferences & Computers and Information in Engineering Conference (IDETC/CIE 2015). DETC2005-85460.

[40] Lee, D.-H., Park, J.-H., Park, S.-W., Baeg, M.-H., and Bae, J.-H., 2017. "KITECH-hand: A

highly dexterous and modularized robotic hand". *IEEE/ASME Transactions on Mechatronics,* **22**(2), pp. 876–887.

[41] Sanchez-Velasco, L. E., Arias-Montiel, M., Guzman-Ramirez, E., and Lugo-Gonzalez, E., 2020. "A low-cost emg-controlled anthropomorphic robotic hand for power and precision grasp". *Biocybernetics and Biomedical Engineering,* **40**(1), pp. 221–237.

[42] Fukaya, N., Asfour, T., Dillmann, R., and Toyama, S., 2013. "Development of a five-finger dexterous hand without feedback control: The TUAT/Karlsruhe humanoid hand". In 2013 IEEE/RSJ International Conference on Intelligent Robots and Systems, pp. 4533–4540.

[43] Mnyusiwalla, H., Vulliez, P., Gazeau, J.-P., and Zeghloul, S., 2015. "A new dexterous hand based on bio-inspired finger design for inside-hand manipulation". *IEEE Transactions on Systems, Man, and Cybernetics: Systems,* **46**(6), pp. 809–817.

[44] You, W. S., Lee, Y. H., Oh, H. S., Kang, G., and Choi, H. R., 2019. "Design of a 3d-printable, robust anthropomorphic robot hand including intermetacarpal joints". *Intelligent Service Robotics,* **12**(1), pp. 1–16.

[45] Kapandji, A., 1986. "Clinical test of apposition and counter-apposition of the thumb". *Ann Chir Main,* **5**(1), pp. 67–73.

[46] Cutkosky, M. R., 1989. "On grasp choice, grasp models, and the design of hands for manufacturing tasks". *IEEE Transactions on Robotics and Automation,* **5**(3), pp. 269–279.

[47] Feix, T., Romero, J., Schmiedmayer, H., Dollar, A. M., and Kragic, D., 2016. "The GRASP taxonomy of human grasp types". *IEEE Transactions on Human-Machine Systems,* **46**(1), pp. 66–77.

APPENDIX A: PARAMETERS FOR THE LINKAGES

In the tables, lengths are in millimetres.

Table 4. Coupled linkage parameters

digit	l_0	l_1	l_2	l_3
Index	33.2	7	36.7	5.48
Middle	38.2	7	41.7	5.48
Ring	38.2	7	41.7	5.48
Little	29.2	7	32.8	5.48
Thumb	39.7	7.38	42.57	5.7

Table 5. Driven linkage parameters

joint	l_0	l_1	l_2	l_3
PIP(all fingers)	25.5	7	27.5	7
MCP-2(Index)	17.6	7	16	10
MCP-2(Ring)	16	7	16	10
MCP-2(Little)	17.6	7	15	10
MCP(Thumb)	13.5	7	15	8.3
CMC-2(Thumb)	16.5	7	21	12.5
CMC-1(Thumb)	14.4	7	13	8

APPENDIX B: D-H PARAMETERS OF THE MCR-HAND II

In the tables, angles are in radian and lengths are in millimetres.

Table 6. D-H parameters of the Thumb

i	α_{i-1}	a_{i-1}	d_i	θ_i
1	$\pi/2$	-20.62	0	0
2	0	0	30.25	θ_{01}
3	$-\pi/2$	-10.66	0	θ_{02}
4	$\pi/2$	44.2	0	θ_{03}
5	0	39.7	0	θ_{04}
6	0	21.2	0	0

Table 7. D-H parameters of the index finger

i	α_{i-1}	a_{i-1}	d_i	θ_i
1	0	0	0	0.364
2	0	-30.07	0	$-\pi/2$
3	0	87.09	0	$-\pi/2-\theta_{11}$
4	$\pi/2$	0	0	θ_{12}
5	0	46.4	0	θ_{13}
6	0	33.2	0	θ_{14}
7	0	25.2	0	0

Table 8. D-H parameters of the middle finger

i	α_{i-1}	a_{i-1}	d_i	θ_i
1	0	0	0	0.364
2	0	-4.07	0	$-\pi/2$
3	$\pi/2$	91.5	0	θ_{21}
4	0	54.4	0	θ_{22}
5	0	38.2.4	0	θ_{23}
6	0	28.2	0	0

Table 9. D-H parameters of the ring finger

i	α_{i-1}	a_{i-1}	d_i	θ_i
1	0	0	0	0.209
2	$\pi/2$	20.13	0	θ_{31}
3	$-\pi/2$	10.24	0	0
4	0	72.64	0	$1.466 + \theta_{32}$
5	$\pi/2$	0	0	θ_{33}
6	0	51.4	0	θ_{34}
7	0	38.2	0	θ_{35}
8	0	25.2	0	0

Table 10. D-H parameters of the little finger

i	α_{i-1}	a_{i-1}	d_i	θ_i
1	0	0	0	0.209
2	$\pi/2$	20.13	0	θ_{41}
3	$-\pi/2$	33.78	0	0
4	0	87.63	0	$1.466 + \theta_{42}$
5	$\pi/2$	0	0	θ_{43}
6	0	42.2	0	θ_{44}
7	0	29.2	0	θ_{45}
8	0	21.2	0	0

APPENDIX C: ABBREVIATIONS USED IN THE KAMAKURA TAXONOMY

The meaning for each of the abbreviations use in the Kamakura taxonomy is listed in table 11.

Table 11. Abbreviations used in the Kamakura taxonomy

Abbreviation	Meaning
PoS	Power grip-Standard type
PoH	Power grip-Hook type
PoI	Power grip-Index finger extension type
PoD	Power grip-Distal type
PoE	Power grip-Extension type
Lat	Lateral grip
T-I	Tripod grip-type I
T-II	Tripod grip-type II
T-III	Tripod grip-type III
PmF	Parallel mild-flexion grip
TiP	Tripod grip
SmF	Surrounding mild-flexion grip
PE	Parallel extension grip
Add	Adduction grip

APPENDIX D: COSTS OF ALL PROTOTYPE COMPONENTS

Table 12. Costs of all prototype components

Components	Price per unit	Quantity	Cost
Hitec HS-5035HD	$24.50	10	$245
MKS DS450	$30.99	7	$216.93
Futaba S3108M	$12.99	1	$12.99
Maestro Controller	$25.95	1	$25.95
Arduino	$16.56	1	$16.56
Printing filament	$20/kg	200g	$4
Others	$10	/	$10
Total			$531.43